Atomistically Modeling the Chemical Potential of Small Molecules in Dense Polymer Microstructures. 1. Method

Birgitta Knopp, Ulrich W. Suter,* and Andrei A. Gusev

Department of Materials, Institute of Polymers, ETH (Swiss Federal Institute of Technology), CH-8092 Zürich, Switzerland

Received March 19, 1997; Revised Manuscript Received July 10, 1997[⊗]

ABSTRACT: A method is presented to estimate the excess chemical potential of solutes in dense polymer microstructures with a combination of the thermodynamic-integration approach and Widom's particle insertion from MD runs under constant *NVT* conditions on an atomistic level. The results obtained for pure water systems show good agreement with other calculated values and with experimental data. The calculated excess chemical potential of water dissolved in a wet polyamide(6) (PA-6) matrix is compared with the corresponding value of pure water. This gives a qualitative estimation of the equilibrium water content of amorphous PA-6.

Introduction

Solution thermodynamics of small molecules in polymeric matrices is a topic of long-standing interest. Especially the solubility of small molecules in dense polymer systems is of great practical importance as evidenced, e.g., by the remarkable dependence of the mechanical properties of polymers on water absorption. The availablity of atomistically detailed structures of the polymeric materials opens up the possibility of investigating the behavior of small molecules in polymer structures. Many such atomistic simulations were carried out in recent years, most of them focused on the calculation of diffusion coefficients and solubilities of simple, nonpolar gases or on structural investigations of cavity sizes and distributions that influence the solubility of small molecules.[1−17]

The solubility of small molecules in polymer matrices depends on the difference in chemical potential between the molecules dissolved in the polymer system and the pure small-molecule system (at equilibrium, the two values are equal). Considering solubility modeling, one has to calculate the chemical potential of the solute, e.g., the water molecules

$$\mu_i = \left.\frac{\partial A}{\partial N_i}\right|_{N_p,V,T} \tag{1}$$

where A denotes the Helmholtz energy of the system, V the volume, T the temperature, and N_i and N_P the number of solute molecules and polymer molecules in the system, respectively. As the ideal part of the Helmholtz energy is straightforward to evaluate, we only consider the excess part of the chemical potential

$$\mu_i^{ex} = \mu_i - \mu_i^{ideal} = \left.\frac{\partial A^{ex}}{\partial N_i}\right|_{N_p,V,T} \tag{2}$$

in our calculations. Excess chemical potentials μ_i^{ex} can be determined from computer simulation by use of the Widom's test-particle-insertion method,[18,19] wherein the excess chemical potential of species i in a (momentarily "frozen") N-particle system is calculated from the potential energy change of the system with N particles i, caused by the insertion of a "test" particle of species i into the system at randomly chosen positions:

$$\mu_i^{ex} = -kT \ln\langle exp[-\Delta U_{pot}^{(N+1;N)}/kT]\rangle_N \tag{3}$$

and k is the Boltzmann factor, T the temperature, and $\Delta U_{pot}^{(N+1:N)}$ the change in the system's potential energy due to the insertion of the test particle. The brackets $\langle ...\rangle_N$ denote the canonical ensemble average over the original system with N particles of type i. This method works very well in many circumstances but runs into difficulties in systems with large solutes or at high density or with strong or long-range interactions, e.g., between dipolar species. Then, inserting a test particle results in the majority of insertions in situations of large positive values of the potential energy. Because of the exponential function in eq 3 these insertions will contribute negligibly to μ_i^{ex} and the method becomes unreliable in these cases. Widom's particle-insertion method is in fact impractical for the calculation of the excess chemical potential of pure water with a density of about 1.0 g/cm^3 (300 K).

The inverse method, in which a real particle is randomly removed from the system, also exhibits problems. In this case the configurations with favorable interaction energies will predominate and this presumably always leads to a systematic underestimation of the true value.[20] In principle, the combination of Widom's insertion method and the inverse method is an attractive alternative,[1,21] but the inverse method has another disadvantage resulting from the fact that each particle can only be removed once from the system, giving poorly converged averages for systems with few solute molecules.

An alternative for the calculation of the excess chemical potential is offered by "thermodynamic integration".[20,22,23] For this method, a function has to be defined that combines the two states of interest as a function of a coupling parameter λ ($0 \le \lambda \le 1$). The difference in Helmholtz energy between the two states ($\lambda = 0$ and $\lambda = 1$), and through it excess chemical potential, if one of the states describes a situation without solute (the solute is an ideal gas), is then expressed as

$$\mu_i^{ex} = \frac{\Delta A^{ex}}{N_i} = \frac{1}{N_i}\int_0^1 \left\langle \frac{\partial U_{pot}(\lambda)}{\partial \lambda}\right\rangle d\lambda \tag{4}$$

where λ is the coupling parameter between the two arbitrary states of the system, N_i is the number of solute molecules, and $U_{pot}(\lambda)$ is the potential energy of the system depending on the coupling parameter λ. The

[⊗] Abstract published in *Advance ACS Abstracts,* September 1, 1997.

S0024-9297(97)00383-5 CCC: $14.00

system is equilibrated for a number of λ states and the derivative of the potential energy with respect to the coupling parameter λ is calculated for each λ. The evaluation of the integral over λ leads to the difference in Helmholtz energy between the two states. Unfortunately, problems arise with this method due to singularities of the derivative of the energy function when the ideal-gas state is approached, since all nonbonded interactions must be annihilated. These problems can be avoided by introduction of a specially designed type of soft-core potential for the nonbonded interactions that approximates the real interaction energies.[24] Nevertheless, it has to be concluded that all standard techniques usually used for the calculation of the excess chemical potential from computer simulations (particle insertion, particle removal, and thermodynamic integration) cannot practically be used in their present form to calculate the excess chemical potential of more complicated solutes such as water in dense polymer microstructures.

Here we present an efficient approach for calculating the excess chemical potential of a solute in dense polymer microstructures, combining two of the well-established methods, thermodynamic-integration and Widom's particle-insertion method. As a test case, we choose water as solute. We will introduce this method and the procedure to obtain the excess chemical potential of water in dense systems in the following sections in detail. We test our method with pure water and show that it is possible to determine the excess chemical potential of water in a dense amorphous microstructure of PA-6 (poly[imino-1-oxohexamethylene]). The comparison of the chemical potentials of water dissolved in the polymer microstructure and of pure water allows then an estimation of the solubility of water in the polymer. The excess chemical potential is simulated here for the different systems in equilibrium, i.e., at the same temperature and pressure (established in *NpT* runs with the same pressure). In this case, the ideal part of the chemical potentials are identical by construction and one needs to consider only the excess parts.

Simulation Method

It is our idea to combine Widom's particle-insertion method and thermodynamic integration to overcome the problems that are associated with the individual methods. To this end and for the case of water, chosen for the purpose of illustration, we define an intermediate state of the system between "real water" and water as an ideal gas, a phase of the latter being the reference state for the excess chemical potential, as schematically depicted in Figure 1. The volume requirements of this intermediate state are reduced by scaling of the nonbonded interactions of the water atoms; therefore, Widom's particle-insertion method becomes more successful with water of this intermediate state. The Helmholtz energy difference between "real" water and the "artificial" water (hereafter termed "noble" water) has still to be calculated, however. This can readily be done with the thermodynamic-integration method. The excess chemical potential of water $\mu^{ex}_{H_2O}$ is obtained, considering Figure 1 and eqs 3 and 4, as

$$\mu^{ex}_{H_2O} = \frac{\Delta A^{ex}_{TI}}{N_{H_2O}} + \mu^{ex}_{WI} \qquad (5)$$

where ΔA^{ex}_{TI} is the difference in Helmholtz energy between real water and noble water, calculated by thermodynamic integration, N_{H_2O} is the number of water molecules in the system, and μ^{ex}_{WI} is the excess chemical potential of the noble water calculated using Widom's particle-insertion method.

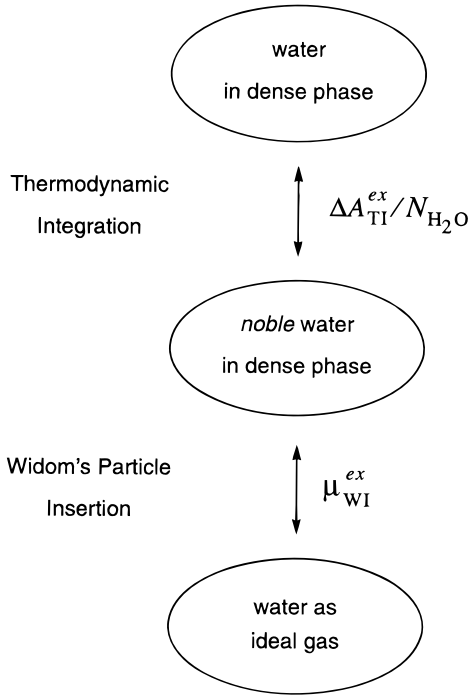

Figure 1. Schematical illustration of the different system states.

The crucial step of the method is the definition of the intermediate state of the water molecules, i.e., of noble water. The main purpose of this intermediate state is to render noble water small enough that the excess chemical potential can be calculated by Widom's particle insertion. Another requirement is obviously that the intermediate state should approximate the ideal gas state "better" than the original system. To this end, all electric field variables, i.e., all partial charges and through them Coulomb interactions with the water molecule, and the nonbonded interactions, i.e., the Lennard-Jones parameters of its hydrogen atoms, are scaled to zero (the force field considered does not include specific hydrogen-bonding terms). Furthermore, the radius of the oxygen atoms of the water molecules is scaled to 80% of its original size. This value was chosen on the basis of preliminary experiments, not presented here, in which we attempted to "optimize" the efficiency of the insertion process. As a result of this scaling, the space needed for a successful insertion of a test particle (a noble water molecule) is significantly smaller than that for a "real" H_2O molecule. For pure water systems, where every molecule is scaled, this results in a considerably larger available space. The definition of the two states is illustrated in Table 1 for clarity.

Following the methodology of thermodynamic integration, we introduce a coupling parameter λ where $\lambda = 1$ denotes real water, and $\lambda = 0$ describes noble water. The manipulation of the interaction parameters of water is shown in Table 2. The λ^2 scaling of ϵ of the hydrogen atoms is one of the simplest functions that avoids a square root of λ in the λ-dependent potential energy originating in the combining rules of the force field.[25] Furthermore, it guarantees an almost linear shape of the derivative of the potential energy with

Table 1. Definition of System States with Dependence on the Coupling Parameter

$\lambda = 1$ "real" water model	$\lambda = 0$ noble water model
all internal interactions	all internal interactions
Coulomb interactions	**no** Coulomb interactions
Lennard-Jones interactions	**no** Lennard-Jones interactions for H atoms **80%** of Lennard-Jones size for O atoms

Table 2. Implementation of λ in the *pcff* Force Field Table[a]

$$U_{\text{pot}} = \epsilon_{ij}\left[2\left(\frac{r_{\text{o},ij}}{r_{ij}}\right)^9 - 3\left(\frac{r_{\text{o},ij}}{r_{ij}}\right)^6\right] + \frac{q_i q_j}{4\pi\epsilon_{\text{o}}\epsilon r_{ij}}$$

$$\text{with} \quad r_{\text{o},ij} = \left[\frac{r_i^6 + r_j^6}{2}\right]^{1/6} \quad \text{and} \quad \epsilon_{ij} = 2\sqrt{\epsilon_i\epsilon_j}\,\frac{r_i^3 r_j^3}{r_i^6 + r_j^6}$$

atom	partial charge q_i	Lennard-Jones interaction parameter r_i	Lennard-Jones interaction parameter ϵ_i
O	$2\lambda q_{\text{org}}$	$(0.8 + 0.2\lambda)r_{\text{org}}$	ϵ_{org}
H	λq_{org}	r_{org}	$\lambda^2\epsilon_{\text{org}}$

[a] The subscript "org" denotes the parameter for "real" water ($\lambda = 1$).

respect to λ, as long as the Coulombic interactions dominate the Lennard-Jones interactions. For water, this condition is fulfilled for $\lambda \geq 0.4$. The form of the resulting potential interaction energy is shown here for the water/water interaction:

$$\tilde{U}_{\text{pot}}(\lambda) = U_{\text{in}} + \lambda^2 U_{\text{el}} + \lambda^2 U_{\text{LJ}}^{\text{HH}} + \tilde{U}_{\text{LJ}}^{\text{OO}}(\lambda) + \tilde{U}_{\text{LJ}}^{\text{OH}}(\lambda) \quad (6)$$

where $\tilde{U}_{\text{pot}}(\lambda)$ is the λ-dependent total potential energy of the system, U_{in} is the (unmodified) potential energy of the internal degrees of freedom, and U_{el} is the electrostatic interaction energy between all atoms; $U_{\text{LJ}}^{\text{HH}}$, $\tilde{U}_{\text{LJ}}^{\text{OH}}$, and $\tilde{U}_{\text{LJ}}^{\text{OH}}$ denote the Lennard-Jones interaction energies for hydrogen−hydrogen, oxygen−oxygen, and oxygen−hydrogen, respectively. The tilde indicates potential energies modified by λ scaling.

Since the thermodynamic-intergration method involves the integration over the derivative of the modified potential energy with respect to the coupling parameter λ (cf. eq 4), it is neccessary to sample $\partial\tilde{U}_{\text{pot}}(\lambda)/\partial\lambda$ in the phase spaces of systems with different λ's and to integrate over λ. We employ nine steps equidistant in λ, between 1 and 0, i.e., a set of 11 force fields with $\lambda =$ 1, 0.9, 0.8, ..., 0. The interaction parameters for water in these force fields are shown in Table 3.

The coupling scheme shown in Table 2 has the advantage that the derivative of the potential energy with respect to λ for pure water systems can be calculated analytically. This leads to the following expression for the derivative of the λ-dependent potential energy

$$\partial\tilde{U}_{\text{pot}}(\lambda)/\partial\lambda = \frac{1}{\lambda}(2\lambda^2 U_{\text{el}} + 2\lambda^2 U_{\text{LJ}}^{\text{HH}}) + \frac{1}{4+\lambda}[9\tilde{U}_{\text{LJ}_{\text{rep}}}^{\text{OO}} - 6\tilde{U}_{\text{LJ}_{\text{disp}}}^{\text{OO}}] + \frac{\mathrm{d}\epsilon_{\text{OH}}(\lambda)}{\mathrm{d}\lambda}\frac{\tilde{U}_{\text{LJ}}^{\text{OH}}}{\epsilon_{\text{OH}}(\lambda)} + \frac{1}{r_{\text{OH}}(\lambda)}\frac{\mathrm{d}r_{\text{OH}}(\lambda)}{\mathrm{d}\lambda}[9\tilde{U}_{\text{LJ}_{\text{rep}}}^{\text{OH}} - 6\tilde{U}_{\text{LJ}_{\text{disp}}}^{\text{OH}}] \quad (7)$$

Thus, we can take all necessary interaction energies for the calculation of the derivative of the potential energy with λ from a standard simulation output.

Table 3. Water Atom Force Field Parameters at Different λ

λ	atom	r_0	ϵ	q
1.0	H	1.0980	0.013 00	+0.3991
	O	3.6080	0.274 00	−0.3991
0.9	H	1.0980	0.010 53	+0.3592
	O	3.5358	0.274 00	−0.3592
0.8	H	1.0980	0.008 32	+0.3193
	O	3.4637	0.274 00	−0.3193
0.7	H	1.0980	0.006 37	+0.2794
	O	3.3915	0.274 00	−0.2794
0.6	H	1.0980	0.004 48	+0.2395
	O	3.3194	0.274 00	−0.2395
0.5	H	1.0980	0.003 25	+0.1996
	O	3.2472	0.274 00	−0.1996
0.4	H	1.0980	0.002 08	+0.1596
	O	3.1750	0.274 00	−0.1596
0.3	H	1.0980	0.001 17	+0.1197
	O	3.1029	0.274 00	−0.1197
0.2	H	1.0980	0.000 52	+0.0798
	O	3.0307	0.274 00	−0.0798
0.1	H	1.0980	0.000 13	+0.0399
	O	2.9586	0.274 00	−0.0399
0.0	H	1.0980	0.000 00	0.0000
	O	2.8864	0.274 00	0.0000

Table 4. Water Atom Force Field Parameters for Numerical Integration of the Derivative $\partial\tilde{U}_{\text{pot}}(\lambda)/\partial\lambda$[a]

	$\lambda = \lambda_0 - 0.01$		$\lambda = \lambda_0 + 0.01$	
λ_0	r_0 (oxygen)	q	r_0 (oxygen)	q
1.0	3.6008	0.3951		
0.9	3.5286	0.3552	3.5431	0.3632
0.8	3.4565	0.3153	3.4709	0.3233
0.7	3.3843	0.2754	3.3987	0.2834
0.6	3.3121	0.2355	3.3266	0.2435
0.5	3.2400	0.1956	3.2544	0.2035
0.4	3.1678	0.1556	3.1823	0.1636
0.3	3.0957	0.1157	3.1101	0.1237
0.2	3.0235	0.0758	3.0379	0.0838
0.1	2.9189	0.0359	2.9658	0.0439
0.0			2.8936	0.0040

[a] ϵ_{H} equals that of the force field at λ_0.

In the case of polymer/water systems, the interactions become formally quite complicated and the derivative of the potential energy with respect to λ is more conveniently computed numerically. This was done by defining two additional force fields with $\lambda \pm \Delta\lambda$ for every λ investigated (where $\Delta\lambda = 0.01$) according to the force field manipulations described in Table 2. The parameters of these additional force fields used to calculated the derivatives of the potential energy are shown in Table 4. The numerical procedure will be checked against the analytical results for the water system in the following section.

Simulation Details

All calculations were performed on IBM RS 6000 or SGI INDIGO workstations using standard molecular dynamics (MD) algorithms (Insight 300/Discover 2.9.7, Biosym/MSI, 1996). Some MD simulations were carried out using Berendsen's thermostat[27] to control the temperature during the data sampling. The equations of motion were integrated with the Verlet leapfrog integrator.[28] The integration time step was set to 1 fs. The *pcff* force field was used to describe the interactions at a fully atomistic level, including internal degrees of freedom for the water molecules and all polymer atoms. The nonbonded interactions, the Lennard-Jones energies and the Coulombic energies, were cut off at 8.5 Å.

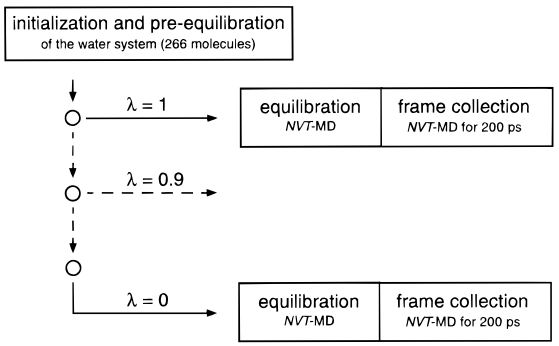

Figure 2. Overview of the MD simulations procedure carried out for the pure water system.

Preliminary studies on PA-6, not described here, had shown that this relatively small cutoff is appropriate for this system, even through it is applied to the long-range Coulombic interactions. These studies had also shown it necessary to reduce the radii of the aliphatic C and H atoms of the Lennard-Jones interactions in the force-field table to $r_C = 3.8897$ and $r_H = 2.9052$ in order to reproduce the density of PA-6 crystals correctly. All simulations were carried out with periodic continuation conditions and the minimum image convention.

The structure of a pure water system with spatial continuation conditions and an edge length of 20 Å containing 266 water molecules was generated at the density of liquid water at 300 K ($\rho = 0.995$ g/cm^3). After 500 steps of steepest-descent minimization of the total potential energy with respect to the coordinates of all atoms, the water structure was preequilibrated for 100 ps by MD simulation under constant *NVT* conditions. The last configuration of this equilibration run was used as the initial configuration for subsequent MD simulations with the different λ-dependent force fields (an alternative procedure, in which the final state of each run at a given λ is used as the initial state for the next smaller λ yields identical results, within the limits of accuracy of the calculation). The structure was further equilibrated up to several hundred picoseconds under constant *NVT* conditions using the different λ-dependent force fields; meanwhile, from 51 to 250 ps, from 296 to 495 ps, from 501 to 700 ps, and from 801 to 1000 ps, respectively, 200 configuration frames of each of the dynamic trajectories were sampled at 1 ps intervals. After each configuration sampling, the convergence of the derivative $\partial \tilde{U}_{pot}(\lambda)/\partial\lambda$ was investigated. Later on, the final 200 configurations were used to evaluate the functional form of the derivative $\partial \tilde{U}_{pot}(\lambda)/\partial\lambda$. The simulation procedure is summarized in Figure 2.

A wet amorphous microstructure of PA-6 was generated with an "*amorphous cell*" procedure[25] at a density of $\rho = 1.09$ g/cm^3 (this is the density of dry amorphous PA-6[26]). This PA-6 system was built of one polymer chain of 50 monomeric units and 35 randomly inserted water molecules, corresponding to 10 wt. % water in the polymer microstructure. After 500 steps of steepest-descent minimization of the total potential energy with respect to the coordinates of all atoms, this structure was first MD-equilibrated for 50 ps under constant *NVT* conditions and then by 350 ps MD simulation under constant *NpT* conditions to adapt the density of the system using Berendsen's method,[27] which couples the system to a pressure "bath" to maintain the pressure at a certain target. During the constant-*NpT* simulation, an external pressure of $p = 1323$ bar was applied to the system in order to compensate for the long-range forces neglected by the cutoff.

Also in the case of the PA-6/water system, the MD simulations in the thermodynamic-integration procedure were carried out by starting each from the last configuration of the equilibration run, analogous to the process shown in Figure 2. Similiar to the water systems, 100 equidistant frames from a 100 ps MD simulation trajectory under *NVT* conditions were collected after 50 ps equilibration time, applying the λ-dependent force fields. In the case of wet PA-6, stimulated by the results of the pure-water simulations, the number of different values of λ was reduced to six, yielding λ-dependent force fields at $\lambda = 1.0$, $\lambda = 0.8$, ..., $\lambda = 0.0$.

In both cases, the pure-water system and the wet PA-6 structure, the frames collected during the MD simulations with $\lambda = 0$ are further used for calculating the excess chemical potential of noble water by use of Widom's particle-insertion method. For this, we divide the simulation box of every configuration into a three-dimensional uniformly spaced grid ($30 \times 30 \times 30$). Insertions at all grid points provide the Boltzmann factor of eq 3 at 27 000 evenly distributed insertion points over the entire box. Tests with finer grids of $50 \times 50 \times 50$ and $100 \times 100 \times 100$ divisions showed no significant change in the resulting excess chemical potential of noble water. More sophisticated methods to enhance the sampling efficiency were not employed, since the computational expense of the insertion procedure is insignificant in comparison to that of generating equilibrated sets of polymer microstructures.

Results and Discussion

Water. As a test, the two-step method for calculating the excess chemical potential of small molecules in dense systems was first applied to pure water. During the first step, thermodynamic integration is used to calculate the difference in Helmholtz energy between neat real water and neat noble water from the derivatives of the potential energy with respect to λ. To this end, the nonbonded energy of the sets of configurations sampled with different λ-dependent force fields (see Figure 2) was calculated. Since only the nonbonded interactions were changed through λ, they contribute alone to the derivatives of the potential energy. These derivatives were estimated by two different methods: (i) numerically, using the finite difference method, and (ii) analytically, where the OO, HH, and OH interactions were used in eq 7 to yield the exact values of the derivative of the potential energy. The analytical results were used to check the accuracy of the numerical approach.

First of all, we looked at the convergence of the derivatives of the potential energy $\partial \tilde{U}_{pot}(\lambda)/\partial\lambda$ for each value of λ, using the numerical estimation of the derivative (see Figure 3). For those force fields with reduced Lennard-Jones interactions of the H atoms but still considerable Coulombic interactions ($\lambda = 0.8$ to $\lambda = 0.4$), the convergence of the derivatives is poor in the first 250 ps MD time (see Figure 3a). For these "intermediate" force fields, the MD simulations had to be extended to 1 ns for the derivatives to converge satisfactorily. The development of the mean derivative $\partial \tilde{U}_{pot}(\lambda)/\partial\lambda$ for each MD run is given in Table 5. For $\lambda = 0$ and $\lambda = 1$, convergence is rapid. It can be seen, however, that even after 1 ns convergence is not complete for some values of λ (e.g., $\lambda = 0.6$). Since the individual results contribute only a minor part to the final (integral) value, it is possible to ignore this residual

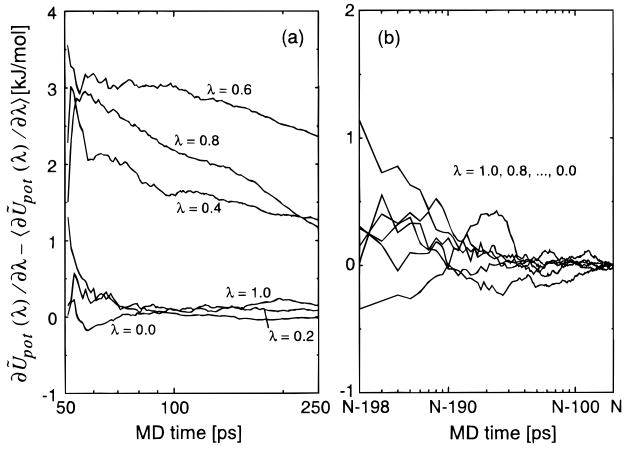

Figure 3. Convergence of the derivative of the potential energy with respect to λ calculated using the MD runs sampled with the λ-dependent force fields: (a) monitored for the configurations sampled between 50 and 250 ps MD time; (b) monitored for the last 200 configurations sampled (see Table 5).

Table 5. Mean Value of $\partial\tilde{U}_{pot}(\lambda)/\partial\lambda$, Numerically Estimated, as a Function of MD Time[a]

λ	50−250 ps	295−495 ps	500−700 ps	800−1000 ps
0.0	+1.0	+1.0(0.1)		
0.1	+2.0	+1.8	+1.9(0.2)	
0.2	−1.0	−1.0	−1.1(0.1)	
0.3	−4.8	−5.2	−5.3	−5.5(0.1)
0.4	−10.5	−11.4	−11.5	−11.7(0.1)
0.5	−17.3	−18.3	−18.9	−19.1(0.1)
0.6	−24.8	−26.0	−26.6	−27.1(0.1)
0.7	−33.2	−34.8	−35.1	−35.2(0.1)
0.8	−41.7	−42.6	−42.7	−42.9(0.1)
0.9	−49.5	−49.9	−50.0	−50.2(0.1)
1.0	−57.3	−57.4	−57.4(0.1)	
$\int_0^1 \left\langle \frac{\partial\tilde{U}_{pot}(\lambda)}{\partial\lambda} \right\rangle d\lambda$	−20.9	−21.6	−21.8	−21.9

[a] The numbers in parentheses give the standard error for the last block of data calculated by presuming uncorrelated data.

deviation from the equilibrium values and to stop the simulation also for the $\lambda = 0.6$ force field. One might speculate that the significant dipolar interactions still present at, e.g., $\lambda = 0.6$, in combination with the high mobility of the already small molecules, cause the very long equilibration times observed.

The Helmholtz energy difference, estimated as integral over the derivative obtained at 11 equidistant λ by the trapezoid rule, is given in the last line of Table 5. The convergence of the individual derivatives from the last 200 ps sampled is shown in Figure 3b. The MD time interval used for the plotted curves is evident from Table 5, where the last column with a numerical entry indicates the interval considered "converged". Those derivatives shown in Table 5 that are not completely converged after 1 ns are possibly still decreasing, and the final value for the Helmholtz energy can be regarded as an upper bound for the excess chemical potential. Further MD sampling will most probably slightly decrease this number. For our purpose, however, its development with sampling time is such that the last value is a sufficient estimate of the Helmholtz energy.

The results obtained by numerical and analytical differentiation of the potential energies of the MD configurations are compared in Figure 4. For all 11 λ values (using 11 different λ-dependent force fields), no

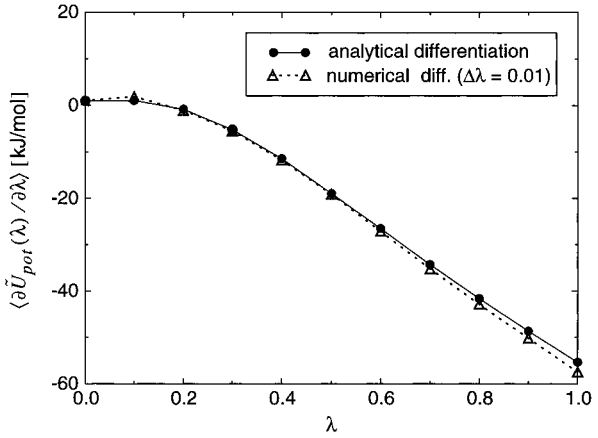

Figure 4. Comparison of the different methods of calculating the derivative of $\tilde{U}_{pot}(\lambda)$ with respect to the coupling parameter λ. Presuming uncorrelated data, the estimated standard error of each MD run with the λ-dependent force fields is within the magnitude of the symbols plotted.

Table 6. Calculated Excess Chemical Potential of Water[a]

	$\Delta A_{TI}/N_{H_2O}$ (kJ/mol)	μ_{WI} (kJ/mol)	μ_{H_2O} (kJ/mol)
analytical (λ interval = 0.1)	−21.4	−1.6	−23.0
numerical (λ interval = 0.1)	−21.9		−23.5
numerical (λ interval = 0.2)	−22.2		−23.8

[a] The difference in Helmholtz energy between liquid water and noble water is calculated using different differentiation methods.

significant differences in the derivatives $\partial\tilde{U}_{pot}(\lambda)/\partial\lambda$ or their dependence on λ could be detected. Both methods show a modestly bent curve of the derivatives, practically linear for $\lambda \geq 0.4$. A minor difference between the two methods can be detected for $\lambda \geq 0.8$. The values of the difference in Helmholtz energy between water and noble water after trapezoidal integration of the points in Figure 4 are listed in Table 6. The numerical estimate is within 3% of that of the analytical approach. In addition, the table lists the result obtained using only six different λ's (six different force fields) at intervals of $\Delta\lambda = 0.2$. It is evident that only a minor difference is introduced through this simplification; the deviation from the analytical result is now less then 4%.

The effect of scaling on the nonbonded energies can be visualized by the changes in the radial pair distribution functions of the center of mass of the H_2O molecules, depicted in Figure 5. For noble water, the peak of the first-neighbor shell of water molecules is shifted to shorter distances since the water molecules do not interact with the hydrogen atoms of the surrounding molecules. Furthermore, the peak of the scaled system is broadend, indicating reduced order in the system; there are no hydrogen bonds in the scaled system that favor specific distances.

In the second step, the remaining part of the total excess chemical potential (eq 5), that of noble water, was calculated by Widom's particle-insertion method. As mentioned above, we insert the noble water test particle on an evenly spaced Cartesian grid of 30 nodes in the *x*, *y*, and *z* directions. The noble water test particle is placed on each grid point in each of the 200 MD configurations, sampled at 1 ps intervals during the MD runs and using the force field with $\lambda = 0$. The resulting 27 000 exponentials (cf. eq 3) for one frame yield one "data point" toward μ_{WI}^{ex}, which is taken as the average over all 200 frames. In Figure 6, the progress of such

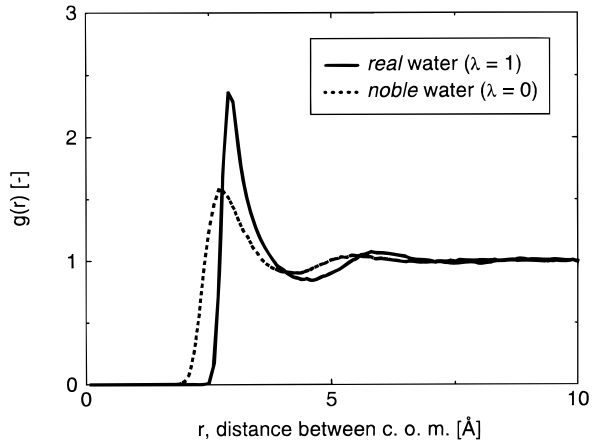

Figure 5. Radial pair distribution functions of the center of mass (C.O.M.) of water molecules for "real" water ($\lambda = 1$) and noble water ($\lambda = 0$), in neat water.

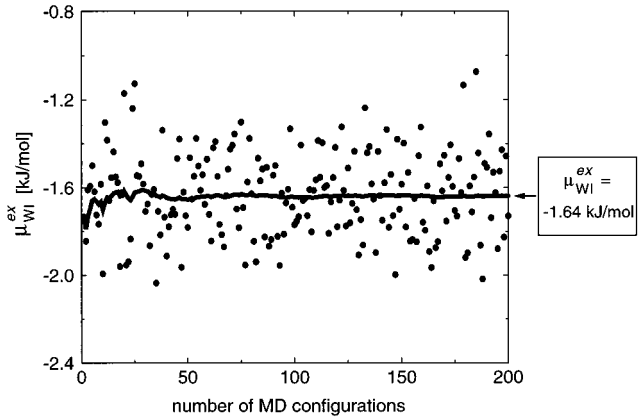

Figure 6. Convergence of the excess chemical potential of noble water calculated by Widom's particle insertion method in 200 configurations (295−495 ps) obtained from the MD simulation using the $\lambda = 0$ force field.

a calculation is displayed using the configurations sampled between 296 and 495 ps of the MD run: each point indicates one application of eq 3 to a frame collected in the sampling run at 1 ps intervals; the line shows the mean value of the resulting chemical potential up to this frame. Convergence of the excess chemical potential of noble water is reached after 30 MD frames, indicating that our noble water system exhibits enough free space for insertion. After 200 frames, $\mu^{ex}_{WI} = -1.6$ kJ/mol. This value is exactly reproduced when the configuration set sampled from 51 to 250 ps MD time is considered. Clearly, configurations of importance in eq 3 occur with sufficient frequency to determine μ^{ex}. The intermediate state, the noble water, was properly chosen.

The excess chemical potential of neat real water is finally obtained by addition of the two intermediate results (see eq 5). Our calculated values (Table 6) show reasonable agreement with other calculated values, obtained by using different atomistic interaction models and different simulation techniques ($\mu^{ex} = -23.4$ to -24.3 kJ/mol)[29−33] and are only slightly different from the experimental value $\mu^{ex} = -23.9$ kJ/mol.[34] The calculated value of the excess chemical potential of water ($\mu^{ex} = -23.8$ kJ/mol) is further used as a reference state to estimate the equilibrium water content of wet polymer microstructures. In a two-phase equilibrium, the chemical potential of water absorbed in a polymer microstructure should be equal to the chemical potential of pure water.

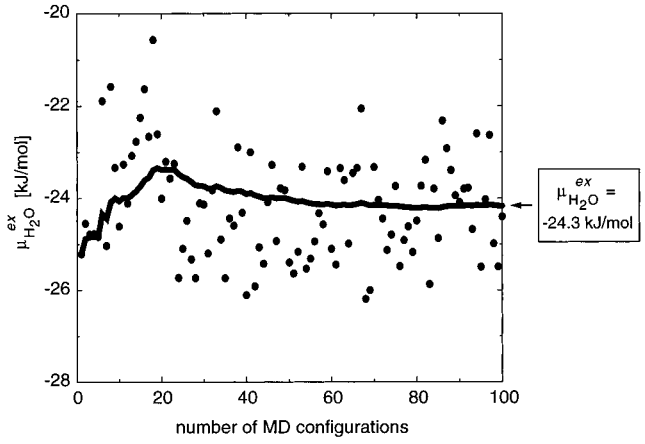

Figure 7. Convergence of the excess chemical potential of water in wet PA-6.

Water in PA-6. We now apply the two-step method to a wet PA-6 system (10 wt. % water content). The MD run procedure outlined in Figure 2 was applied, in analogy to the pure-water system, to the final configuration of a 400 ps MD equilibration run under constant NpT conditions. Using the configuration sets of the trajectories obtained from the MD runs with different λ-dependent force fields, we calculate the difference in Helmholtz energy of real water dissolved in PA-6 and noble water dissolved in PA-6 to $\Delta A^{ex}_{TI}/N_{H_2O} = -26.3$ kJ/mol. Widom's particle insertion of a noble water test particle in the configurations collected on a 30 × 30 × 30 grid with the force field of $\lambda = 0$ gave the excess chemical potential of noble water in PA-6 as $\mu^{ex}_{WI} = +2.0$ kJ/mol, with a convergence more rapid than that for pure water. The two intermediate results add to an estimated excess chemical potential of water dissolved in PA-6 at 10 wt. % of $\mu^{ex}_{H_2O} = -24.3$ kJ/mol. The convergence of this result with the number of sampled MD configurations is depicted in Figure 7; every individual point in this figure is the sum from the result of thermodynamic integration and 27 000 Widom's insertions on the current MD frame. The line drawn is the running average over the points.

The probable error of the final excess chemical potential can be estimated to about ±0.15 kJ/mol using the blocking method for correlated data.[35] Of course, this small error refers to a single microstructure and does not take into account any variation between microstructures; the correlation times of structural relaxations are much longer[9] than our simulation time, and processes of the polymer backbone such as transitions in the skeletal torsion angles were not observed during the MD runs. One might argue that the solubility must be influenced mainly by the size and distribution of "cavities" in the system and the details of the polymer packing (and, hence, the variations between structures) essential for the chemical potential; we will report on such investigations elsewhere.

Because our simulations show that the excess chemical potential of water dissolved in a polymer matrix at a level of 10 wt. % ($\mu^{ex}_{H_2O} = -24.3$ kJ/mol) is lower than that of pure water, $\mu^{ex} = -23.8$ kJ/mol (calculated using numerical differentiation, six λ-dependent force fields, see Table 6), we conclude that amorphous PA-6 with 10 wt. % water favors the absorption of further water molecules from pure water. This result agrees with the experimental data of the equilibrium water content of PA-6: Semicrystalline PA-6 shows an equilibrium water

content (submerged in water) of about 10 wt %,[26] which, taking into account that only the amorphous phase is able to absorb water molecules significantly,[36] leads to an estimated equilibrium water content of about 15% for purely amorphous PA-6.

Conclusion

Our simulations demonstrate that it is possible to combine thermodynamic integration and Widom's particle-insertion method in order to calculate the excess chemical potential of liquid water and of water dissolved in dense polymer microstructures. This two-step method is appropriate to estimate whether an amorphous polymer is able to absorb a given amount of water.

Furthermore, our two-step method exhibts advantages in comparison to other approaches for the estimation of the solubility of gases. It allows us to obtain structural information from the MD runs, which is impossible for some other methods that produce biased trajectories, e.g., umbrella sampling. It can easily be implemented in general modeling software, the only changes required being in the force fields corresponding to the "intermediate" state. There is a great deal of flexibility in the definition of the scaling functions.

The estimation of the equilibrium water content of amorphous polymers could proceed through applying the procedure to "wet" microstructures containing different numbers of water molecules. Since we have used no restrictions specific to PA-6, a transfer of this method to other polymer systems containing water molecules is straightforward and we will show results in the companion paper.[37] It seems further possible to use our two-step method quite generally to calculate chemical potentials of small molecules and perhaps of small oligomers in dense systems. The only prerequisite seems to be an appropriate scaling of the nonbonded interactions in such a manner that Widom's particle-insertion method, possibly with the assistance of more sophisticated sampling methods,[21,36] becomes feasible. We cannot, at present, give a general recipe for the construction of "universal" scaling functions that will give correct results with high efficiency; nevertheless, the approach presented is highly promising.

Acknowledgment. We gratefully acknowledge support for B.K. from the Deutsche Forschungsgemeinschaft under Grant No. DFG Kn 417/1-1 and general financial support by EMS-Chemie AG, Domat/Ems, Switzerland. Generous amounts of computer time were provided by the Competence Centre for Computational Chemistry (C4) of the ETH Zürich.

References and Notes

(1) Shing, K. S.; Gubbins, K. E. *Mol. Phys.* **1981**, *43*, 717.
(2) Takeuchi, H.; Okazaki, K. *J. Chem. Phys.* **1990**, *92*, 5643.
(3) Takeuchi, H.; Roe, R.-J.; Mark, J. E. *J. Chem. Phys.* **1990**, *93*, 9042.
(4) Mueller-Plathe F. *Macromolecules* **1991**, *24*, 6475.
(5) Gusev, A. A.; Suter, U. W. *Phys. Rev. A* **1991**, *43*, 6488.
(6) Sok, R. M.; Berendsen, H. J. C.; van Gunsteren, W. F. *J. Chem. Phys.* **1992**, *96*, 4699.
(7) Pant, P. V.; Boyd, R. H. *J. Chem. Phys.* **1993**, *98*, 9895.
(8) Gusev, A. A.; Arizzi, S.; Suter, U. W.; Moll, D. J. *J. Chem. Phys.* **1993**, *99*, 2221.
(9) Gusev, A. A.; Suter, U. W. *J. Chem. Phys.* **1993**, *99*, 2228.
(10) Mueller-Plathe, F.; Rogers, S. C.; van Gunsteren, W. F. *J. Chem. Phys.* **1993**, *98*, 9895.
(11) Han, J.; Boyd, R. H. *Macromolecules* **1994**, *27*, 5365.
(12) Tamai, Y.; Tanaka, H.; Nakanishi, K. *Macromolecules* **1994**, *27*, 4498.
(13) Tamai, Y.; Tanaka, H.; Nakanishi, K. *Macromolecules* **1995**, *28*, 2544.
(14) Gee, R. H.; Boyd, R. H. *Polymer* **1995**, *36*, 1435.
(15) Gusev, A. A.; Suter, U. W.; Moll, D. J. *Macromolecules* **1995**, *28*, 2582.
(16) Ralston, A. R. K.; Denton, D. D.; Bicerano, J.; Moll, D. *Comput. Polym. Sci.* **1996**, *6*, 15.
(17) Bicerano, J. Moll, D. J. *Comput. Polym. Sci.* **1996**, *6*, 117.
(18) Widom, B. *J. Chem. Phys.* **1963**, *39*, 2808.
(19) Widom, B. *J. Phys. Chem.* **1982**, *86*, 869.
(20) King, P. M. In *Computer Simulations of Biomolecular Systems*; van Gunsteren W. F., Weiner, P. K., Wilkinson, A. J., Eds.; ESCOM: Leiden, 1993; Vol. 2, pp 267−314.
(21) de Pablo, J. J.; Laso, M.; Suter, U. W. *Macromolecules* **1993**, *26*, 6180.
(22) Kirkwood, J. G. *J. Chem. Phys.* **1935**, *3*, 300.
(23) van Gunsteren, W. F.; Beutler, T. C.; Fraternali, F.; King, P. M.; Mark, A. E.; Smith, P. E. In *Computer Simulations of Biomolecular Systems*; van Gunsteren W. F., Weiner, P. K., Wilkinson, A. J., Eds.; ESCOM: Leiden, 1993; Vol. 2, pp 315−348.
(24) Beutler, T. C.; Mark, A. E.; van Schaik, R. C.; Gerber, P. R.; van Gunsteren, W. F. *Chem. Phys. Lett.* **1994**, *222*, 529.
(25) Insight 3.0.0; Discover 2.9.7; Amorphous Cell 8.0.0; Biosym/MSI, Inc., San Diego, CA, 1996.
(26) *Polymer Handbook*, 3rd ed.; Brandrup, J., Immergut, E. H., Eds.; Wiley: New York, 1989.
(27) Berendsen, H. J. C.; Postma, J. P. M.; van Gunsteren, W. F.; DiNola, A.; Haak, J. R. *J. Chem. Phys.* **1984**, *81*, 3684.
(28) Verlet, L. *Phys. Rev.* **1967**, *159*, 98.
(29) Hermans, J.; Pathiaserli, A.; Anderson, A. *J. Am. Chem. Soc.* **1988**, *110*, 5982.
(30) Jorgensen, W. J.; Blake, J. F.; Buckner, J. K. *Chem. Phys.* **1989**, *129*, 193.
(31) Watanabe, M.; Reinhardt, W. P. *Phys. Rev. Lett.* **1990**, *65*, 3301.
(32) Mezei, M. *J. Comput. Chem.* **1992**, *13*(5), 651.
(33) Fay, P. J.; Ray, J. R.; Wolf, R. J. *J. Chem. Phys.* **1994,** *100*, 2154.
(34) Sarkisov, G. H.; Dashevsky, V. G.; Malenkov, G. G. *Mol. Phys.* **1974**, *27*, 1249.
(35) Flyvbjerg, H.; Petersen, F. G. *J. Chem. Phys.* **1989**, *91*, 461.
(36) Song, J.; Ehrenstein, G. W. *Kunststoffe* **1990**, *80*, 722.
(37) Knopp, B.; Suter, U. W. *Macromolecules* **1997**, *30*, 6114.
(38) Leontidis, E.; Suter, U. W. *Mol. Phys.* **1994**, *83*, 489.

MA970383U